Surfaces and Interfaces 26 (2021) 101417

Contents lists available at ScienceDirect

Surfaces and Interfaces

journal homepage: www.sciencedirect.com/journal/surfaces-and-interfaces

Scrutinizing the importance of surface chemistry versus surface roughness for aluminium / sol-gel film adhesion

U. Tiringer [a,b,*], J.P.B. van Dam [a,1], S.T. Abrahami [c], H. Terryn [c], J. Kovač [d], I. Milošev [b], J.M. C. Mol [a]

[a] Delft University of Technology, Department of Materials Science and Engineering, Mekelweg 2, 2628 Delft, CD, The Netherlands
[b] Jožef Stefan Institute, Department of Physical and Organic Chemistry, Jamova c. 39, SI-1000 Ljubljana, Slovenia
[c] Department of Materials and Chemistry, Research Group Electrochemical and Surface Engineering (SURF), Vrije Universiteit Brussel, Pleinlaan 2, B-1050 Brussels, Belgium
[d] Jožef Stefan Institute, Department of Surface Engineering and Optoelectronics, Jamova c. 39, SI-1000 Ljubljana, Slovenia

ARTICLE INFO

Keywords:
Pre-treatment
Aluminium
Surface chemistry
Surface morphology
Wettability
Sol-gel
Coatings
Interface
Adhesion

ABSTRACT

The sol-gel synthesis process is a versatile method used to produce a wide diversity of materials and is being increasingly used as a surface modification method to alter porosity, wettability, catalytic activity, biocompatibility and corrosion performance of underlying substrates. Silane sol–gel films deposited on aluminium and aluminium alloys have been widely studied as chemical conversion coatings and as coupling agent between the substrate and organic layers. This study set out to investigate the effect of the surface chemical treatment prior to sol-gel application on the interfacial adhesion properties of a hybrid sol-gel film. Different surface pre-treatments, including two abrasive treatments and three chemical surface pre-treatments were used and their effect on surface chemistry and surface roughness was assessed. Surfaces were characterized by scanning electron microscopy, x-ray photoelectron spectroscopy, roughness measurements and static contact angles. Cerium nitrate loaded hybrid sol-gel films were deposited and adhesion on commercially pure aluminium was evaluated using pull-off testing. Statistical analysis revealed that, although highest adhesion values were obtained on rougher surfaces, the strongest correlation exists between the surface hydroxyl fraction and adhesion strength.

1. Introduction

A versatile method used to produce a wide diversity of materials is the sol-gel synthesis process [1]. The materials created by this process range from inorganic glasses to complex organic-inorganic hybrid (OIH) materials. Sol-gel synthesis is therefore being increasingly used as a surface modification method to alter porosity, wettability, catalytic activity, biocompatibility and corrosion performance of the underlying substrate [2]. It is this versatility of materials and applications that has generated great interest in the application of the sol-gel technique to develop thin films and coatings [3].

Organic-inorganic hybrid (OIH) sol-gel materials are based on organic and inorganic precursors and thus combine both the advantages of organic polymers (i.e. impact resistance, flexibility and light weight) and of their inorganic constituents (chemical resistance, thermal stability and mechanical strength) [4]. Silicon alkoxide precursor-based OIH sol–gel materials provide additional attractive properties in terms of adhesion promotion of organic films to metallic substrates, as well as providing corrosion protection [5,6]. For this reason they are commonly regarded as suitable replacement for toxic chromate (VI) conversion coatings and have been the topic of many investigations in the last decades [7,8]. Even though these type of sol-gel films were developed to promote the interaction and adhesion between metallic substrates and organic resins [9,10], up to now research on this topic has tended to focus on the barrier- and anti-corrosion properties of these sol-gel films. Numerous studies have focussed on the effect of the chemical constituents and the preparation conditions on the physical properties of sol-gel films, as well as the effect of doping agents to provide active corrosion protection to a large arrangement of aluminium alloys [11–17]. However, to date, little investigation has been carried out on the application of sol-gel films on commercially pure aluminium (Al) and AA1xxx aluminium alloys [15,18–21].

* Corresponding author.
E-mail address: U.Tiringer-1@tudelft.nl (U. Tiringer).
[1] These authors have equally contributed to the manuscript.

https://doi.org/10.1016/j.surfin.2021.101417
Received 4 November 2020; Received in revised form 10 August 2021; Accepted 11 August 2021
Available online 27 August 2021

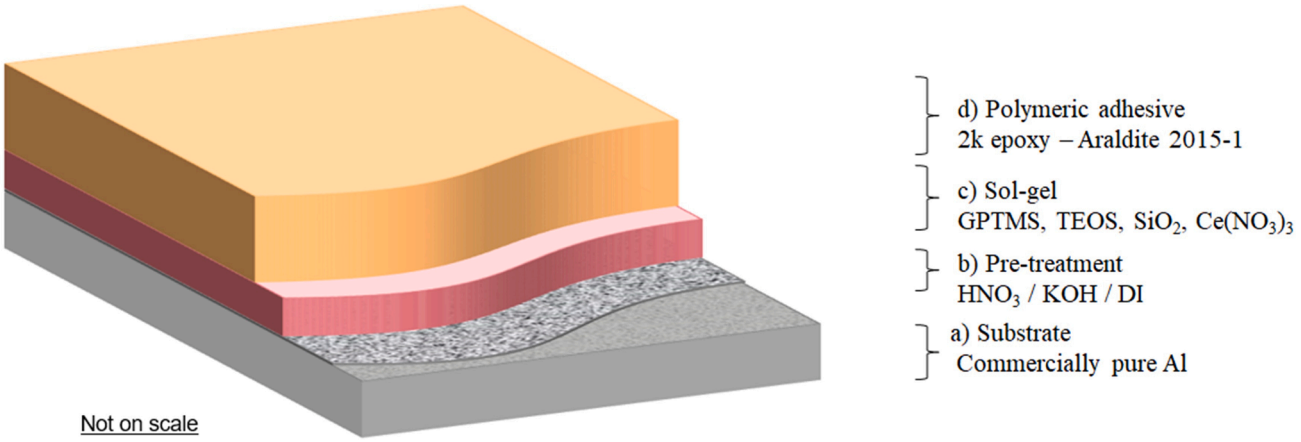

Fig. 1. Schematic representation of the system studied in this work, with (a) the base substrate, (b) the pre-treatment layer, (c) the sol-gel coating and (d) the polymeric adhesive.

Fedel et al. conducted several studies on the application of OIH sol-gel coatings on AA1XXX alloys and showed that both the interfacial adhesion and barrier properties of the films are highly dependent on the ratio of chemical constituents [20,22,23]. A separate study was devoted to investigate the effect of three different surface pre-treatments on the physical and electrochemical barrier properties of the sol-gel films [24]. It was found that the surface chemistry, in particular the type of oxide present at the aluminium surface, is of great influence on the formation mechanism and kinetics of the gelating sol. In particular, the formation of a superficial pseudoboehmite layer, AlO(OH), after a boiling water treatment, led to a decreased number of defects, improved homogeneity and increased stability of the metal surface/sol–gel coating interface. An explanation for this evidence relies on the efficient interactions between the hydroxyl groups of the pseudoboehmite and the Si-OH groups of the silanols, leading to the formation of dense networks.

The mechanism through which siloxane-based sol-gel films are bonding to metallic surfaces is usually explained by a scheme introduced by Arkles et al., where interfacial bonding is assumed to proceed subsequently via hydrogen bonding, a condensation reaction and covalent bonding (Al-O-Si) to surface hydroxyl groups [25]. This reaction mechanism between siloxane-based precursors and oxidized Al surfaces was recently studied by DFT calculations by Poberznik et al., who confirmed the energetically favourably mono- and bidentate formation after condensation reaction between alkoxysilanes and y-AlO(OH) surfaces [26].

Marcoen et al. performed a systematic TOF-SIMS study on the bonding mechanism between alkoxysilanes and steel surface hydroxides and successfully observed the conversion of hydrogen bonds to covalent bonding interactions through a condensation reaction promoted by curing [27].

Together, these studies indicate that interfacial interactions occur through the surface hydroxyls and therefore, the type and number of surface interactions between substrate and sol-gel, as well as the formation kinetics/mechanism of the sol-gel film is highly dependent on substrate surface conditions. Despite this, solely the role of the aluminium/sol-gel interface on the adhesion promoting properties of the sol-gel has not been a topic of investigation yet.

Therefore, this study set out to investigate the role of physico-chemical surface properties of commercially pure Al on the adhesive properties of TEOS-GPTMS silane precursor-based hybrid sol-gel coatings. Commercially pure Al was chosen to exclude possible effects of laterally varying surface morphology and chemistry due to heterogeneously distributed intermetallics present in commercial grade structural Al alloys. Three different chemical surface pre-treatments and two grades of abrasion were employed to alter surface chemical composition and surface texture. Subsequently, adhesion was investigated between an epoxy-based adhesive and commercially-pure Al substrates using pull-off testing. Statistical analysis is used to investigate and correlate the dependence of the wetting behaviour of the aluminium substrate and the subsequent adhesion of applied sol-gel films on the induced changes to surface properties.

2. Experimental

2.1. Sample base materials and surface preparation

Fig. 1 presents an illustration of the studied sample configuration. It consists of the base substrate covered by three distinct layers: the pre-treated surface, sol-gel and polymeric adhesive. Each consecutive layer application process is individually described in a separate section below.

2.2. Substrate and surface preparation

Commercially pure (c. p.) Al was supplied by Goodfellow with a purity of 99.999 wt % of Al and 0.001 wt % of other trace elements.

Half of the Al samples were mechanically abraded with SiC paper up to 4000 grit and the other half up to 800 grit, from now on referred to as ‘4000 grit’ and ‘800 grit’, respectively. After grinding, all samples were ultrasonically cleaned in ethanol for 10 minutes to remove physically adsorbed organic contaminations from the surface and dried with nitrogen gas.

Reference samples without subsequent pre-treatment are labelled as ‘bare’. In order to modify the surface chemistry, three different pre-treatments were applied on priorly mechanically abraded substrates to alter the surface oxide chemistry and superficial hydroxyl fraction; acidic, alkaline and boiling water treatment [28]. The acid treatment consisted of a 30 s immersion in 30 vol% HNO_3 (pH 0.1), the alkaline treatment involved a 3 min immersion in a 3 vol% KOH solution at 57 ℃ (pH = 10.8) and for the boiling water treatment, substrates were immersed for 15 s using boiling deionized water (pH = 7.2). After each treatment, samples were rinsed with deionized water and dried with nitrogen gas.

2.3. Sol-gel synthesis and deposition

The formulation of the hybrid sol-gel used in the present work is based on our earlier work [13]. The sol-gel was prepared by mixing tetraethoxysilane (TEOS, Aldrich, 99%), 3-(glycidyloxypropyl)trimethoxy silane (GPTMS, ABCR, 98%) and colloidal silica SiO_2 (Ludox-4S, Aldrich, aqueous suspension 40 wt%). Cerium nitrate ($Ce(NO_3)_3.6\ H_2O$, Aldrich, 98%) was added to the formulation as active corrosion

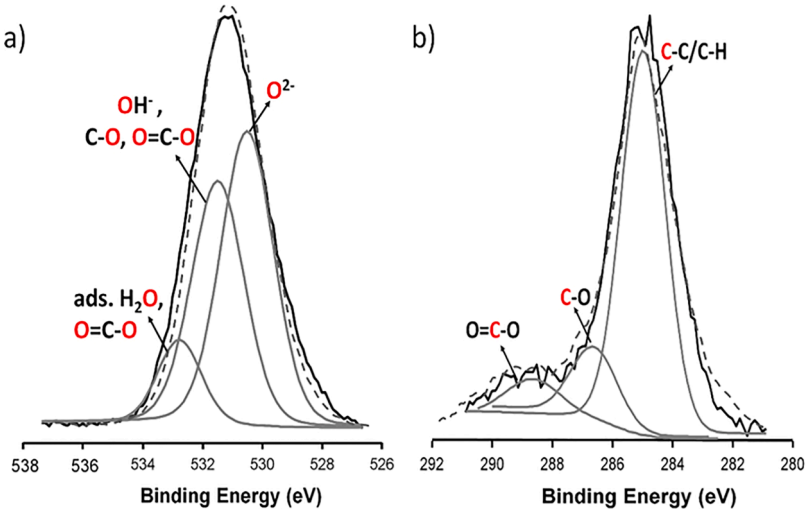

Fig. 2. XPS high resolution spectra of Al pre-treated with HNO_3 showing peaks used for a) O 1s and b) C 1s peak fitting, these peaks are labelled with grey solid curves. The dashed curve represents the sum of fitted peaks and the solid black curves are the measured peaks.

Table 1
Constraint parameters applied for curve fitting the O 1s and C 1s Multiplex XPS peaks.

O 1s			C 1s		
Component	FWHM (eV)	Relative position lock (eV)	Component	FWHM (eV)	Relative position lock (eV)
O^{2-}	1.80–1.84	0	*CC/CH*	1.6	0
OH^-	1.68–1.72	1.1–1.2	*CO*	2.0	1.5
H_2O	2.03–2.07	2.43	*COO*	1.4–2.0	3.8–4.3

inhibitor. After 30 min of stirring, 0.6 mL of concentrated HNO_3 (VWR, 65%) was added as a catalyst for polycondensation. Finally, absolute ethanol (EtOH, Panreac, 99.8%) was added as a solvent. The molar ratio of the sol was TEOS/GPTMS/SiO_2/Ce = 0.5/0.5/0.54/0.03, denoted as GTS-Ce.

GTS-Ce sol was applied on the differently pre-treated substrates by dip-coating. Dip-coating is performed with a withdrawal rate of 30 cm/min and samples were subsequently thermally treated for 1 h at 120 °C to complete the polymerization between sol and Al substrate. The thickness of the sol-gel layer is 3.4 ± 0.5 μm [11].

2.4. Polymer adhesive application

The adhesive used in this work is a two-part epoxy system, Araldite® 2015-1 from Huntsman Advanced Materials (Switzerland) GmbH. This is a DGEBA based structural epoxy adhesive. Mixing of the two components was done using an adhesive application gun equipped with a mixing nozzle to control a 1:1 ratio. Curing was performed for 24 h at room temperature, in line with the application data sheet supplied by the manufacturer.

2.5. Characterization methods

General microscopic observations related to the morphology of the differently pre-treated Al samples, after 800 grit and 4000 grit grinding, were obtained by scanning electron microscopy, performed on a JEOL IT100 Scanning Electron Microscope (SEM). Images of pre-treated surfaces were obtained at a magnification of one thousand five hundred at an acceleration voltage of 10 kV and were processed with JEOL's InTouchScope™ software.

Oxide surface chemistry of differently pre-treated Al samples was studied by X-ray photoelectron spectroscopy (XPS). To exclude the effect of surface roughness in the quantification of the chemically modified OH fraction, XPS analysis was carried out on finely abraded samples (4000 grit). As previously shown by van den Brand et al., the OH fraction is angle-dependent [29]. Hence, increasing the surface roughness from 4000 grit to 800 grit will affect OH quantification by changing the orientation of the incident X-ray angle. Despite the increase in total surface area induced by the rougher abrasion (800 grit), the relative OH fraction is assumed to be unaffected as it is a direct result of the same subsequent chemical modification as for the 4000 grit [30].

XPS analysis was carried out using a PHI-TFA XPS spectrometer (Physical Electronic Inc.), equipped with an x-ray Al-monochromatic source. The vacuum during XPS analysis was 10^{-9} mbar. The analysed area was 0.4 mm in diameter and the depth of analysis was 3–5 nm. Narrow multiplex scans of the peaks were recorded using a pass energy of 23.5 eV with a step size 0.1 eV, at a take-off angles of 45 ° with respect to the sample surface. Low energy electron gun was used for surface charge neutralization XPS. Spectra were processed using Multipak v. 8.0 (Physical Electronics Inc.). Three XPS spectra were recorded for each sample, at different spots and the elemental composition was determined from the XPS survey spectra.

High-energy resolution spectra of O 1s and C 1s photoelectron peaks were curve-fitted to quantify the relative amounts of hydroxyls at the surface of Al after the different pre-treatments. Fig. 2 presents fitted spectra of O 1s (a) and C 1s (b) of Al pre-treated with HNO_3, as an example. The rest of the fitted spectra are not shown but were obtained in a similar manner.

Curve-fitting was carried out with a deconvolution of the oxygen peak into three components: O^{2-}, OH^- and adsorbed H_2O (Fig. 2a) and the carbon peak into the C-C/C-H, CO and COOX components (Fig. 2b), using the constraint parameters that are listed in Table 1 [31].

The percentage of hydroxyls on each pre-treated substrate was calculated using an extended model based on the one developed by McCafferty and Wightman [32]. Mathematical details concerning curve-fitting and calculation of the relative OH concentration are presented in previous work [29,31,33,34]. In short: the fitted intensity areas were used to find a solution for the amount of O^{2-}, OH^- and H_2O, while taking into account the intensity originating from oxygen species with overlapping binding energies coming from atmospheric contamination. These are provided by the intensities of the fitted C-O and O=C-O sub peak areas in C 1s (Fig. 2). The relative percentage of OH^- was then determined by the ratio presented in Eq. (1).

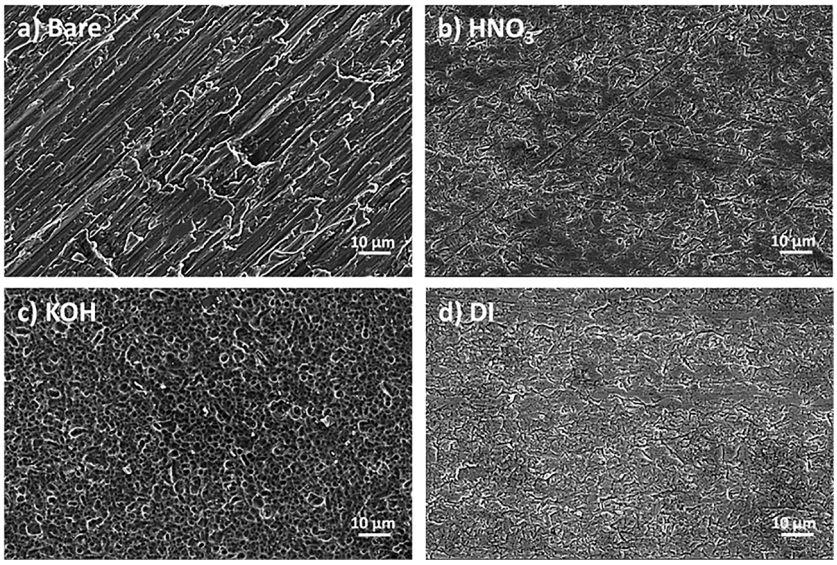

Fig. 3. SEM images of (a) bare Al (4000 grit) and Al (4000 grit) pre-treated with (b) HNO_3, (c) KOH and with (d) boiling DI water. The SEM images were taken in secondary electron imaging (SEI) mode.

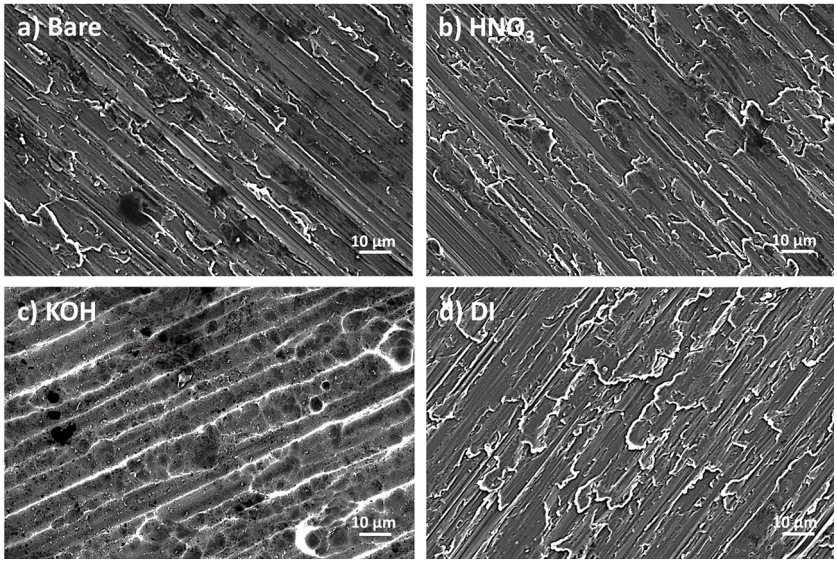

Fig. 4. SEM images of (a) bare Al (800 grit) and Al (800 grit) pre-treated with (b) HNO_3, (c) KOH and with (d) boiling DI water. The SEM images were taken in secondary electron imaging (SEI) mode.

$$OH^- \ (\%) = \frac{c_{OH^-}}{c_{OH^-} + c_{O^{2-}} + c_{H_2O}} \text{x } 100 \quad (1)$$

The surface topography was analysed with a Bruker DektakXT profilometer. The instrument has a lateral resolution of 1 µm and a resolution of 5 nm perpendicular to the surface plane. Measurements were performed for a 1 mm × 2 mm surface area. The data were processed with TalyMap Gold 6.2 software, using ISO 25178, to create a 3D surface topography and to calculate the arithmetic surface roughness (S_a), skewness (S_{sk}), kurtosis (S_{ku}), maximum height (S_z) and root mean square height (S_q). Each parameter is calculated from three measurements at three different spots on the surface. All calculated roughness parameters of 800 grit and 4000 grit samples after different pre-treatments are presented in Appendix (Tables A.1, A.2).

To test the wettability of the differently pre-treated samples, static water contact angles were recorded using Easy Drop Standard system Kruss DSA 100 equipment. If recorded water contact angles (CA) are below 90 °, the surface is considered hydrophilic and the wettability of the solid as high, while for contact angles above 90 °, the surface is considered hydrophobic and the wettability is regarded as poor [35]. Measurements on each sample were performed in threefold.

The adhesion between differently pre-treated Al samples and the subsequently applied sol-gel and adhesive was measured using a pull-off adhesion test. The pull-off adhesion tests were performed using an Elcometer® 106 Pull-Off Adhesion tester, according to ASTM D4541- 17. Dollies of 20 mm in diameter were attached to the samples using Araldite *2015-1* and cured for 24 h at room temperature. The bond line thickness was controlled to be 300 µm using glass beads supplied by Sigma Aldrich. The dollies were pulled off at a pull-rate of 0.20 MPa per second. All tests were performed in threefold to allow evaluation of reproducibility and calculation of average adhesion failure strengths (pull-off strengths) and standard deviations.

Table 2
Elemental surface composition obtained from XPS spectra after different pre-treatments of commercially pure Al.

Pre-treatment	O [at %]	C [at %]	Al [at %]	N [at %]	Ca [at %]	Si [at %]
4000 grit Bare	47.0	36.8	10.8	2.6	1.4	1.4
HNO_3	47.6	35.6	16.8	/	/	/
KOH	44.8	43.5	11.1	/	/	0.6
DI	62.0	21.3	16.7	/	/	/

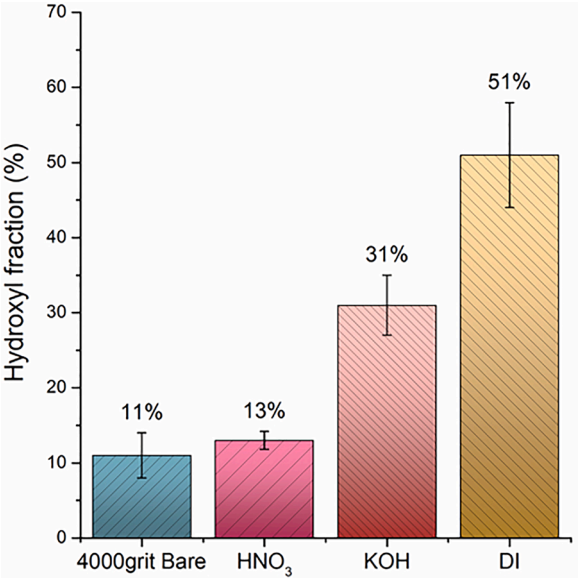

Fig. 5. Hydroxyl surface fraction for 4000 grit bare and differently pre-treated Al.

2.6. Statistical analysis

In order to evaluate the performance of different pre-treatments with respect to OH fraction, S_a, CA and adhesion, we compared them with the baseline scenario – bare (before any pre-treatment and without sol-gel coating). This performance was defined as the relative increase (%) shown in the Eq. (2):

$$Relative\ increase\ (\%)_{i,j} = \frac{x_{i,j} - x_{bare,\ j}}{x_{bare,j}} \quad (2)$$

Where *i* represents the type of the pre-treatment and j = OH / S_a / CA / adhesion and x represents the obtained value of j after each i. Relative increases were calculated for 4000 grit and 800 grit samples. Individual values and calculated relative increases are present in the Appendix, Table A.3.

In order to compare the contribution of OH fraction on the adhesion versus the contribution of Sa on the adhesion, the relative increases of S_a and OH versus adhesion are depicted (Fig. 9).

In order to determine correlations between the OH fraction, roughness (Sa), water contact angles (CA) and adhesion, a Pearson's correlation analysis (r) Eq. (3) and p-value significance Eq. (4) was used.

$$r_{xy} \frac{\sum_{i=1}^{n}(x_i - \bar{x})(y_i - \bar{y})}{\sqrt{\sum_{i=1}^{n}(x_i - \bar{x})^2 \sum_{i=1}^{n}(y_i - \bar{y})^2}} \quad (3)$$

Where *n* is the sample size and x_i and y_i are the individual values of the compared pairwise parameters (OH fraction, S_a, CA and adhesion).

$$p - value = r_{xy} \sqrt{\frac{n-2}{1-r^2}} \quad (4)$$

A strong pairwise correlation is considered to be present if $r_{xy} \geq 0.7$ and *p*-value < 0.01 [36,37].

3. Results and discussion

3.1. General observations

General observations considering the surface morphology of differently pre-treated c.p. Al substrates, after 800 grit and 4000 grit grinding, obtained by scanning electron microscopy are shown in Figs. 3 and 4.

The surface of bare 4000 grit Al is rough and layered, with a directional pattern being observed (Fig. 3a). The pattern consists of scratches and rolling lines, which are a direct result from prior mechanical processing and abrasion. After subsequent wet pre-treatments; HNO_3 (Fig. 3b), KOH (Fig. 3c) and boiling DI water (Fig. 3d), the surface pattern of Al alters. HNO_3 pre-treatment causes layers of Al to disappear and the surface pattern is more uniform compared to bare Al (Fig. 3a). In addition, acidic pre-treatment with HNO_3 revealed a scalloped appearance. This pattern is a result of the high acidity (pH 0.1) of HNO_3 at which Al is uniformly dissolved [38]. Some scratch marks are still present and are the result of grinding. The surface of Al after KOH treatment shows a distinctively different morphology compared to the other surfaces. Due to the pH of KOH being 10.8, Al is dissolved in the form of $[Al(OH)_4]^-$ / $[AlO_2]^-$, resulting in a uniform pattern of micro- and nano-scale round-shaped pores. The surface of Al after DI pre-treatment is similar to the surface pre-treated with HNO_3, with an even more scalloped pattern (Fig. 3d), characteristic for pseudoboehmite [AlO(OH)] formation on the Al surface [28,33,34]. Moreover, the temperature of DI water is 100 °C which may cause dissolution of Al and result in the additional scalloped pattern.

The surface of bare 800 grit Al is rough and layered, with a similar directional pattern being observed (Fig. 4a) as for the bare 4000 grit (Fig. 3a). The pattern consists, beside scratches and rolling lines, of black stains which are the result of aggressive grinding. After subsequent wet pre-treatments, HNO_3 (Fig. 4b), KOH (Fig. 4c) and boiling DI water (Fig. 4d), the surface morphology does not appear to change as much as for the 4000 grit specimens. The pattern of 800 grit Al after KOH pre-treatment is most similar to the one obtain for 4000 grit Al after KOH. Thus, the pre-treatment has a high effect on the morphology of 4000 grit Al surface, while this effect is much lower for rougher 800 grit Al surfaces. To sum up, the morphology of commercially pure Al is overall dominated by roughness intrinsically present and not by chemistry, caused by pre-treatment. This is further confirmed and elaborated in "Surface roughness" section.

3.2. Surface chemistry

The elemental composition in the near-surface region and surface oxide chemistry of differently pre-treated Al, after 4000 grit grinding, were determined by XPS analysis. Table 2 shows a qualitative comparison of the surface chemical composition for the differently pre-treated Al, as obtained from XPS survey spectra (Appendix, Figs. A.1–A.4). As expected, the major elements for the bare substrates are O, C and Al. The detection of oxygen is related with the Al oxide layer formed at the surface, while the detection of C can be attributed entirely to the presence of ambient contamination, i.e. adventitious carbon [32]. On the bare Al and the Al after KOH pre-treatment, additional minor traces of N, Ca and Si were detected (Table 2). They are considered to be the result of contamination, originating from the handling and grinding process. The highest concentration of O was detected after boiling DI water pre-treatment, demonstrating the thickest oxide formation and indicating possible Al_2O_3 formation, which could be related with the pH of DI boiling water (7.2) at which Al is in the form of pseudoboehmite [29,34].

No additional elements, related with the surface pre-treatments, were detected at the surface of differently pre-treated Al. Thus, apart

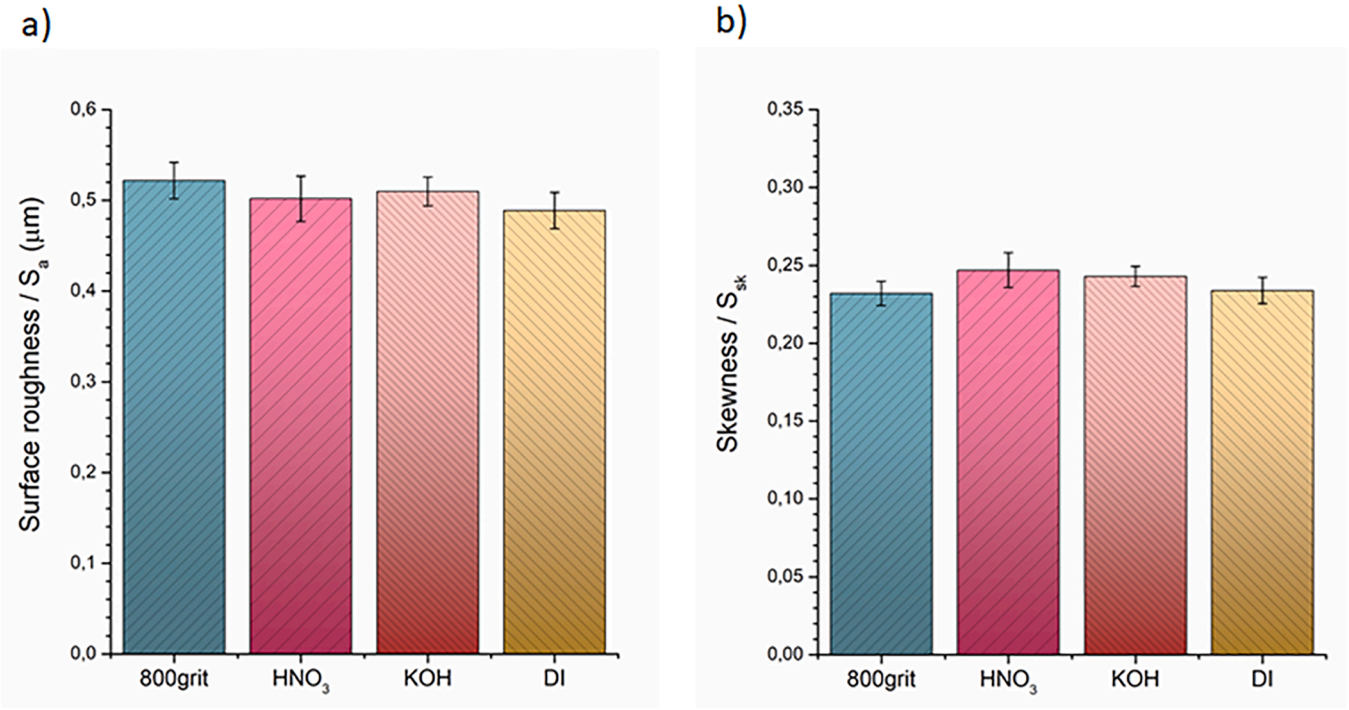

Fig. 6. The 3D (a) arithmetic roughness, S_a and (b) skewness, S_{sk}, of differently pre-treated commercially pure Al, ground up to 4000 grit.

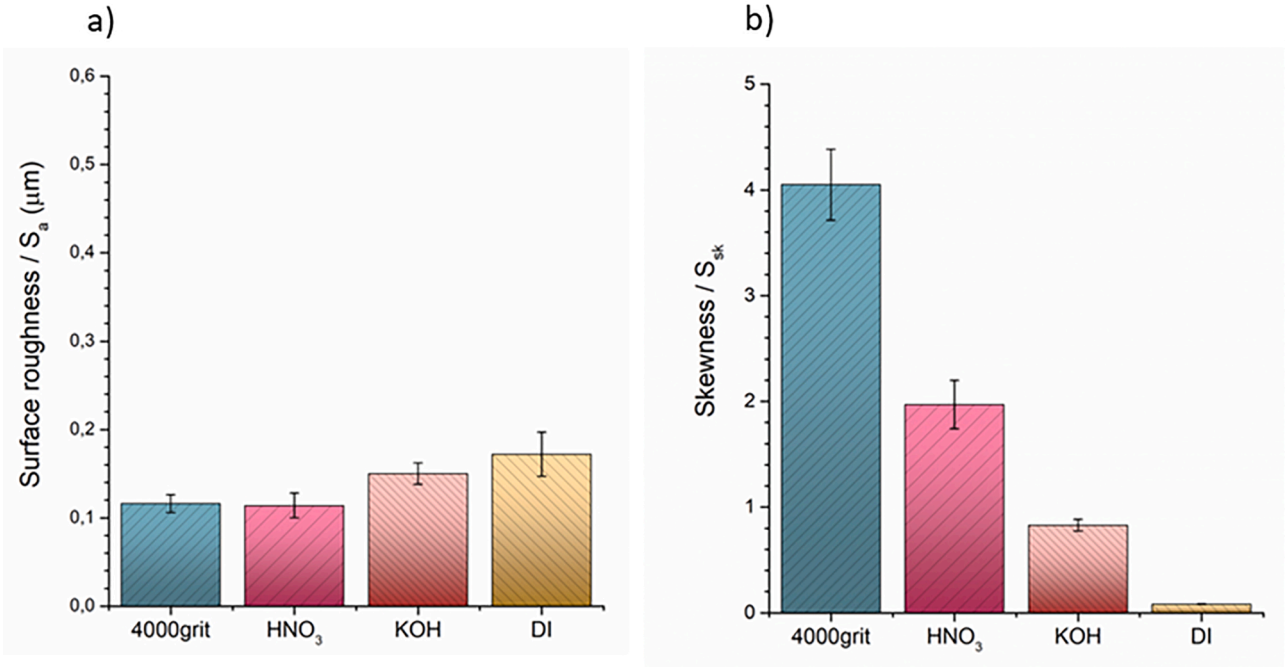

Fig. 7. The 3D (a) arithmetic roughness, S_a and (b) skewness, S_{sk}, of differently pre-treated commercially pure Al, ground up to 800 grit.

from oxide formation it can be concluded that the pre-treatments do not impose additional alterations to the surface chemical composition of commercially pure Al.

As described in the experimental section, hydroxyl fractions were derived from the XPS spectra by peak-fitting of the high-energy O 1s and C 1s photoelectron peaks. The average binding energies (BE) of the fitted subpeaks in O 1s are the following: BE (H_2O) = 532.9 (± 0.17) eV, BE (OH^-) = 531.7 (± 0.23) eV and BE (O^{2-}) = 530.5 (± 0.14) eV. The average binding energies (BE) of the fitted subpeaks in C1s are the following: BE (COO) = 288.5 (± 0.20) eV, BE (CO) = 286.4 (± 0.14) eV and BE (CC) = 284.8 (± 0.11) eV. Fig. 5 shows the average values of OH fractions obtained for the differently pre-treated Al samples. A negligible increase is noticed between bare Al (11%) and HNO_3 treated Al (13%), while after KOH pre-treatment the OH fraction of Al increase to 31%, and after DI boiling water to 51%. The lowest hydroxyl fractions were observed for the bare Al and for Al pre-treated with HNO_3. Pre-treatment based on KOH significantly increased the hydroxyl fraction of Al as a result of [Al(OH)4]– formation [38]. However, the highest hydroxyl

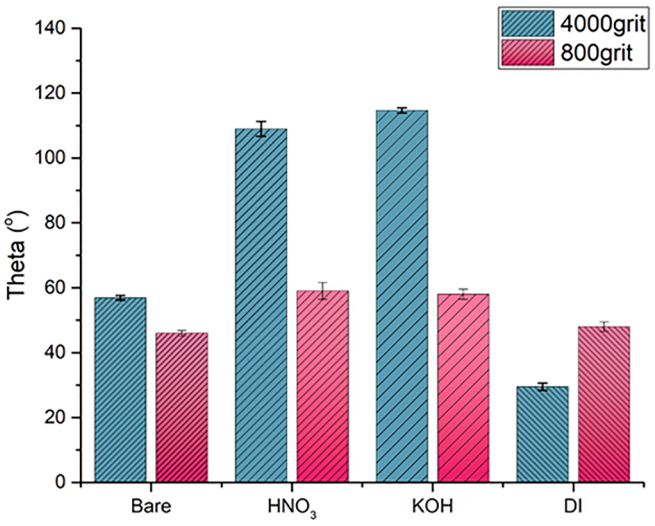

Fig. 8. Water contact angles (theta) of differently pre-treated commercially pure Al, ground up to 4000 grit and up to 800 grit.

fraction of commercially pure Al was observed after boiling water pre-treatment, due to pseudoboehmite [AlO(OH)] formation which is in accordance with the literature [29,33,34].

Furthermore, XPS spectra of Al 2p also show Al-oxide and Al-metallic peaks for bare Al and Al pre-treated with HNO_3 which means that the Al-oxide layer was about 1-3 nm thick [39]. For Al pre-treated with KOH and boiling water no Al-metallic peak was observed, meaning that the Al-oxide layer was thicker than 5 nm (Appendix, Fig. A.5) [39]. These findings confirm that alkaline and boiling water pre-treatment react more aggressively with commercially pure Al.

3.3. Surface roughness

Surface roughness measurements were performed with a stylus profilometer to assess any significant variations and changes in the surface roughness of commercially pure Al as a result of the pre-treatments. Many roughness parameters can be used to measure or express the roughness of a surface, of which S_a, the arithmetic mean height of the 3D roughness, is the one most commonly used [40]. Nevertheless, the S_a in itself is insufficient to evaluate the topography of a surface. The skewness parameter (S_{sk}) provides additional information about the distribution of the varying heights of the roughness profile and allows for a description of the roughness profile along with the S_a. A full description of all roughness parameters is provided in the Supplementary information.

The arithmetic roughness and skewness values of differently pre-treated Al are presented in Fig. 6. For the bare 4000 grit Al, roughness is ~ 0.12 μm. The difference of S_a after HNO_3 pre-treatment is negligible, while after KOH pre-treatment the roughness significantly increases (S_a ~ 0.15 μm). After boiling DI water the increase of S_a is even higher (0.17 μm). Thus, the trend of S_a is the following: bare 4000 grit < HNO_3 < KOH < boiling DI (Fig. 6). Hence, the roughness exhibits a similar trend as the calculated hydroxyl surface fraction, (Fig. 6) and a higher roughness corresponds to a higher degree of surface texturing observed in SEM (Fig. 3).

Furthermore, the surface of commercially pure Al after all treatments exhibits a positive skewness, indicating a non-normal height distribution representative for a surface with more peaks than valleys. The bare 4000 grit Al exhibits the highest skewness of around 4.0. Subsequent treatment of the Al substrate results in a decrease of the skewness to more moderate values, ranging from 0.1 (DI) to 2.0 (HNO_3). From these Fig.s it can be concluded that the subsequent wet treatments of Al result in a

Table 3
Pearson pairwise correlation coefficients (r) for all variables of 4000 grit and 800 grit Al.

Pearson correlation coefficient (*r*)	S_a	OH	Adhesion	CA
S_a	1	0.1	0.6	-0.5
OH (4000 grit)	0.1	1	0.7	-0.3
Adhesion	0.56	0.7	1	-0.2
CA	-0.5	-0.3	-0.2	1

Table 4
p-value of pairwise of all variables of 4000 grit and 800 grit Al.

p-value	S_a	OH	Adhesion	CA
S_a	/	0.40	$5.65{\cdot}10^{-9}$	$8.74{\cdot}10^{-7}$
OH (4000 grit)	0.42	/	$2.69{\cdot}10^{-11}$	$1.76{\cdot}10^{-4}$
Adhesion	$5.65{\cdot}10^{-9}$	$2.69{\cdot}10^{-11}$	/	$2.68{\cdot}10^{-3}$
CA	$8.74{\cdot}10^{-7}$	$1.76{\cdot}10^{-4}$	$2.68{\cdot}10^{-3}$	/

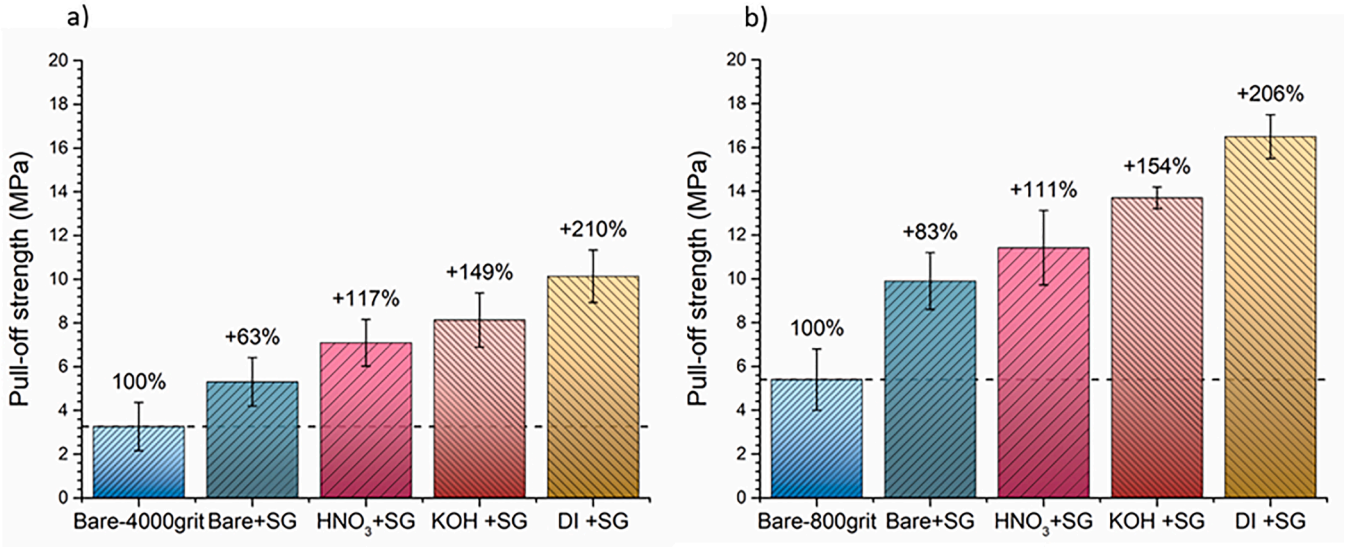

Fig. 9. Average adhesion strength (pull-off strength) of differently pre-treated commercially pure Al, ground up to (a) 4000 grit and up to (b) 800 grit. On all substrates epoxy based adhesive Araldite was deposited. SG refers to the pre-application of a sol-gel coating.

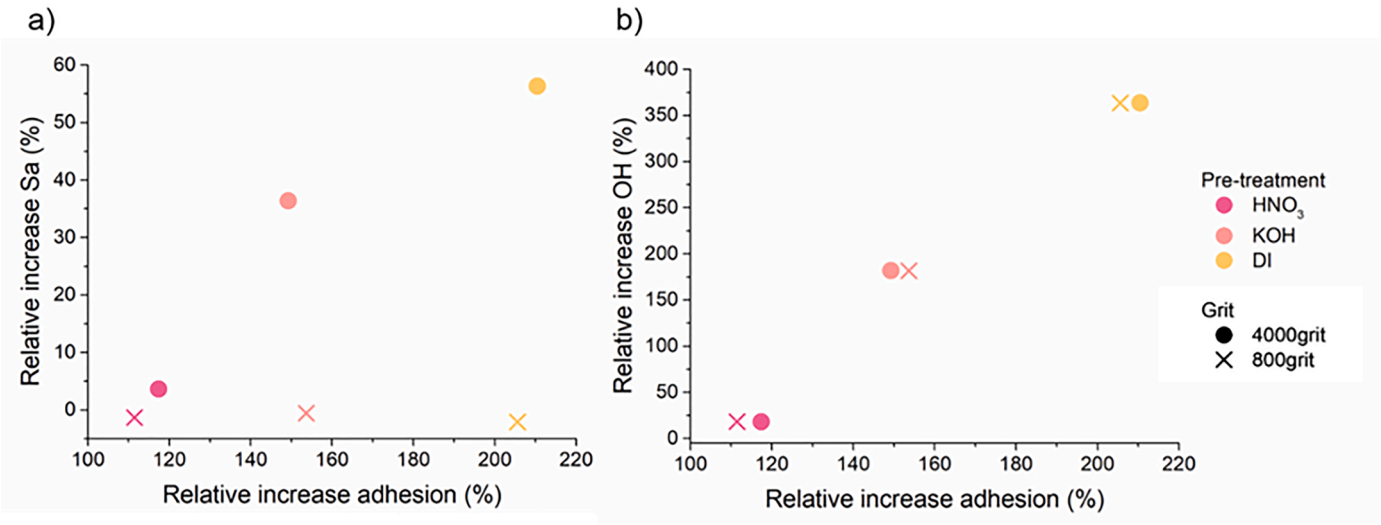

Fig. 10. Relative increases of (a) S_a versus adhesion and (b) OH versus adhesion.

Table A.1
Roughness parameters of 4000 grit Al after different pre-treatments.

Roughness parameter [μm]	4000 grit	HNO_3	KOH	DI
S_a	0.116	0.114	0.150	0.172
S_q	0.170	0.168	0.206	0.229
S_z	2.43	2.72	2.86	3.02
S_{sk}	4.05	1.97	0.829	0.0821
S_{ku}	13.8	18.6	21.5	6.73

Table A.2
Roughness parameters of 800 grit Al after different pre-treatments.

Roughness parameter [μm]	800 grit	HNO_3	KOH	DI
S_a	0.522	0.502	0.510	0.489
S_q	0.671	0.651	0.699	0.702
S_z	6.10	6.21	6.34	6.54
S_{sk}	0.232	0.247	0.243	0.234
S_{ku}	3.81	3.79	3.74	3.63

decrease of the skewness and therefore more normal height distributions along the roughness profile.

Since at the constant 4000 grit roughness (0.12 μm) the trend for the calculated hydroxyl fraction and roughness is similar after different pre-treatments of Al, it would be impossible to distinguish between the contributions of these two individual parameters to the wettability and adhesion. Therefore, an additional set of Al samples was ground up to 800 grit and the 3D roughness was measured again under the same conditions (Fig. 7). Presenting much rougher surface conditions, all S_a values were higher compared to the 4000 grit specimens (Fig. 6). For the bare 800 grit the roughness is over four times higher than the 4000 grit, with S_a around 0.52 μm. After all subsequent pre-treatments no significant roughness change is noticed.

The skewness for the bare 800 grit is 0.23 and pre-treated Al surfaces have similar skewness values around 0.24. So, for the skewness a similar absence of alteration as for the arithmetic roughness is observed, with all skewness values being very close to zero, i.e. much lower than for 4000 grit specimens (Fig. 6). The skewness describes a symmetric normal distribution of the roughness before and after all treatments. Therefore, unlike in the case of finely abraded Al specimens (4000 grit), it is clear from these roughness measurements that the pre-treatments induce non-significant morphological changes to the surface of commercially pure Al when the surface was initially rough (800 grit) (Figs. 6, 7). This finding is in accordance with SEM images (Figs. 3, 4) where it was shown that the morphology is overall dominated by roughness intrinsically present and not by chemistry, caused by pre-treatment.

3.4. Wettability

The effect of pre-treatment and roughness on wettability of commercially pure Al was evaluated by measuring the static water contact angles (CA) on differently pre-treated Al surfaces, after abrasion up to 4000 and 800 grit (Fig. 8). The surface of 4000 grit bare Al is hydrophilic with a water contact angle of 57°. After subsequent HNO_3 and KOH pre-treatment the water contact angle of Al doubles and the surface becomes hydrophobic, while after boiling water pre-treatment the water contact angle decreases (30 °) compared to the bare 4000 grit Al and the surface becomes more hydrophilic.

However, water contact angles of the rough Al samples are lower and all 800 grit Al surfaces are hydrophilic after pre-treatments. The water contact angle of bare 800 grit is 46° and after HNO_3 and KOH it increases to 59°. After boiling water treatment the water contact angle is similar to

Table A.3
Obtained values (S_a, CA, OH and adhesion) and corresponding relative increases of fine (4000 grit) and rough (800 grit) Al before and after pre-treatment.

Sample	S_a [μm]	Rel.increase [%]	CA []	Rel.increase [%]	OH [%]	Rel.increase [%]	Adhesion [MPa]	Rel.increase [%]
4000 grit	0.11	0.0	56.9	0.0	11.0	0.0	3.3	0.0
HNO_3	0.11	3.6	109.0	91.6	13.0	18.2	7.1	117.4
KOH	0.15	36.4	114.7	101.6	31.0	181.8	8.1	149.2
boiling DI	0.17	56.4	29.5	-48.2	51.0	363.6	10.1	210.5
Sample	**S_a [μm]**	**Rel.increase [%]**	**CA []**	**Rel.increase [%]**	**OH [%]**	**Rel.increase [%]**	**Adhesion [MPa]**	**Rel.increase [%]**
800 grit	0.52	0.0	46.0	0.0	11.0	0.0	5.4	0.0
HNO_3	0.52	-1.3	59.0	28.3	13.0	18.2	11.4	111.5
KOH	0.52	-0.6	58.0	26.1	31.0	181.8	13.7	153.7
boiling DI	0.51	-2.1	48.0	4.3	51.0	363.6	16.5	205.6

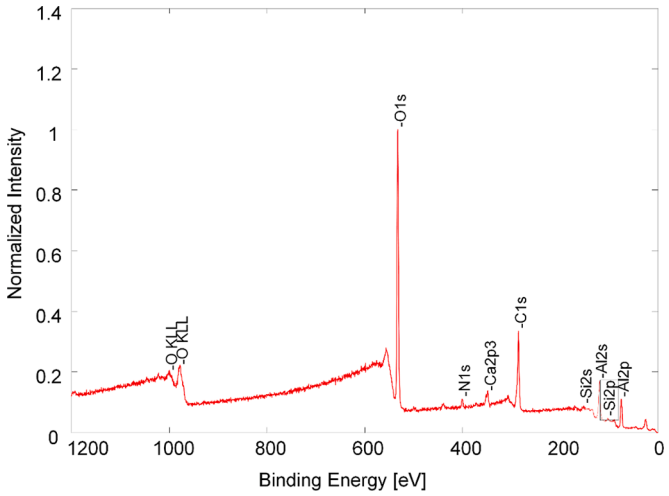

Fig. A.1. Survey XPS spectrum of bare Al (4000 grit).

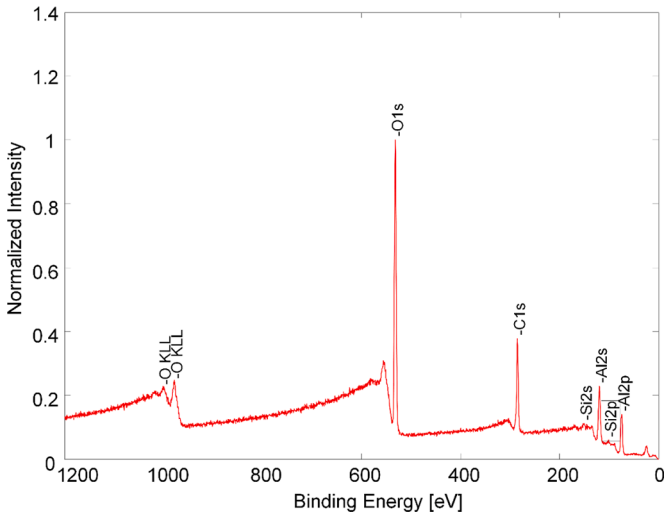

Fig. A.2. Survey XPS spectrum of Al pre-treated with HNO_3.

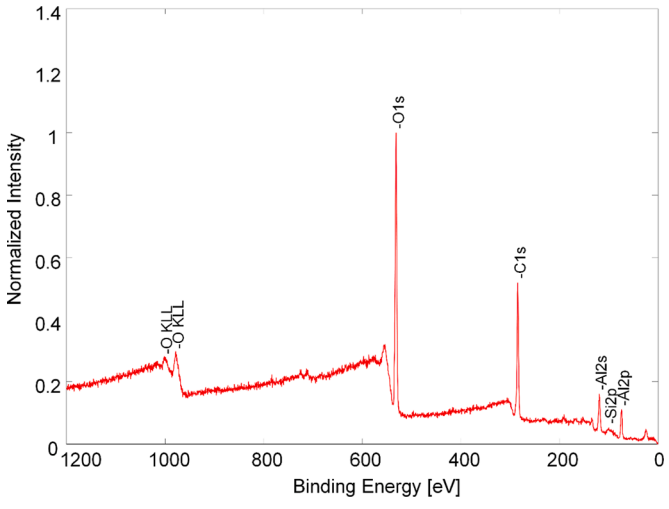

Fig. A.3. Survey XPS spectrum of Al pre-treated with KOH.

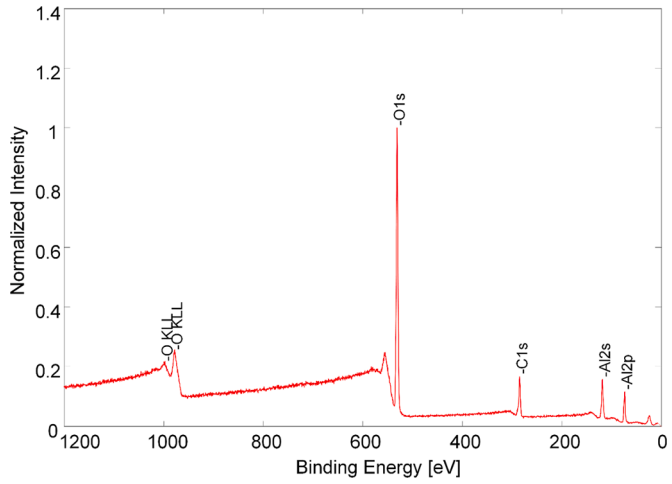

Fig. A.4. Survey XPS spectrum pre-treated with boiling DI water.

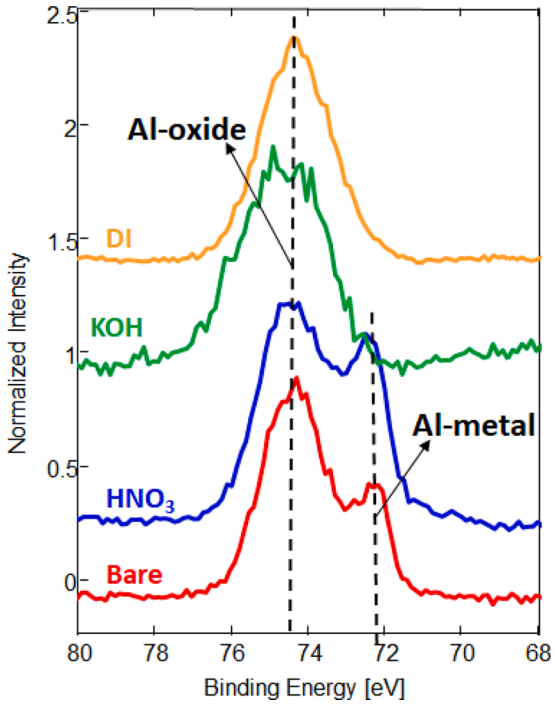

Fig. A.5. High resolution XPS spectra of Al 2p, recorded for differently pre-treated c. p. Al.

the bare 800 grit. The overall hydrophilicity of the rougher surfaces (800 grit) is due to the fact that more water can penetrate into the rougher texture, resulting in smaller water contact angles [41]. This is in accordance with the Wenzel model, indicating penetration of the surface texture by the liquid [42].

Although the trend of water contact angles for the rougher (800 grit) and finely (4000 grit) abraded pre-treated samples is similar (indicating that surface pre-treatment and its effect on the surface chemistry have a significant effect on surface wettability), the relative changes are not in the same order.

The higher water contact angles after HNO_3 and KOH pre-treatments on 4000 grit samples could be related to fine micro-pore patterning on the Al surface (Fig. 3 b,c). This enables surrounding air to be trapped inside textural features, forming an isolating layer of air, resulting in reduced wetting or water adsorption. This describes a Cassie state or 'Lotus effect' which is in accordance with the Cassie-Baxter model [43].

Although the morphology of the Al surface after boiling DI water pre-treatment is similar to the HNO_3 treated surface, the evolution of the water contact angle does not exhibit the same trend. This is due to the higher wettability of the relative oxides present on the surface, pseudoboehmite versus Al_2O_3, respectively [30]. Since the effect of pre-treatments on pattern of 800 grit Al surface in lower after HNO_3 and KOH pre-treatments (Fig. 4 b, c), the water contact angles does not increase as much, after these two pre-treatments, as for 4000 grit Al.

3.5. Adhesive bonding

The effect of chemistry, roughness and wettability of the different pre-treated surfaces on the adhesion of a hybrid sol-gel coating was evaluated by measuring the pull-off strengths. Sol-gel coatings were applied on the four different substrates (bare, HNO_3, KOH and boiling water) and dollies were adhered using the epoxy-based adhesive with 300 μm bondline thickness. Bare samples, without pre-treatment after abrasion, were tested as a reference. The results are summarized in Fig. 9.

For bare 4000 grit reference the average pull-off strength is 3.3 MPa. After sol-gel application this value increases by 61% to 5.4 MPa, showing a significant effect of sol-gel coating on adhesion, which is in accordance with literature (Fig. 9a) [10,44]. After HNO_3, KOH and boiling water pre-treatment, followed by sol-gel application, the obtained pull-off strengths are, respectively 117%, 149% and 210% higher. The highest pull-off strength was obtained after boiling DI water pre-treatment, which is in a good agreement with previous findings (OH, S_a, CA) and can be related to the formation of a pseudoboehmite layer [33,45].

In order to distinguish between roughness and hydroxyl fraction effect, surfaces with higher roughness and same pre-treatments were assessed in terms of adhesion (Fig. 9b).

The pull-off strength of the bare 800 grit reference sample is 5.4 MPa, which is higher compared to bare 4000 grit Al. After sol-gel application adhesion increases by 83% compared to the reference. After HNO_3, KOH and boiling water pre-treatment, relative increases in the adhesion are, respectively 112%, 154%, 224%. Adhesion values of rougher, 800 grit Al samples follow the same trend and relative increases in adhesion compared to the smoother 4000 grit substrates. This effect is observed despite of the absence of significant topographical changes of differently pre-treated Al surface ground at 800 grit (as derived from the SEM images in Fig. 4 and roughness measurements in Fig. 7).

The results show that the application of sol-gel coating increases the adhesion with the epoxy-based adhesive for fine (4000 grit) and rough (800 grit) bare Al substrates. Furthermore, all pre-treatments lead to an additional increase of the adhesion strength. Since the trend of the adhesion of 4000 grit and 800 grit Al sample is very similar, the improved adhesion can be predominantly assigned to the altered surface hydroxyl fraction. However, the roughness still plays an important role provided that all adhesion values of 800 grit samples are higher compared to the 4000 grit. However, it can be concluded that the water contact angle and adhesion are not directly related, provided the trend in adhesion values do not follow the trend in wettability /hydrophilicity. This confirms that the obtained surface wettability is predominantly governed by the surface morphology (roughness) and texture (for 4000 grit Al), thereby repressing possible effects induced by surface chemistry. In contrast, it can be concluded that the surface chemistry is an important determinant of the interfacial adhesion strength.

3.6. Statistical analysis

As discussed in the sections above, one of the goals of the present work was to investigate the relative contributions of hydroxyl fraction and roughness on the wettability and adhesion for differently pre-treated Al samples.

In order to conclude whether the obtained results show significant differences and to determine the correlations between all measured variables (OH fraction, S_a, CA and adhesion), a complementary statistical analysis was performed. Pearson's correlation coefficient matrix (r) and p-value statistics were used and the obtained values are presented in Tables 3 and 4, respectively. Over all the measured samples, including both the smooth (4000 grit) and rough (800 grit) surfaces, a significant pairwise correlation was found for OH and adhesion indicated by $r = 0.7$ and a p-value of 12.69^{-11}, which is « 0.01. A similar correlation was found between S_a and adhesion with $r = 0.6$ and the p-value $5.65 \cdot 10^{-9}$. A negative non-significant pairwise correlation was found for CA and OH (r = -0.3), S_a (r = -0.5) and adhesion (r = −0.2), with p-values of $1.76 \cdot 10^{-4}$, $8.74 \cdot 10^{-7}$ and $2.68 \cdot 10^{-3}$, respectively.

Based on the statistical analysis performed on all measured samples it can be concluded that both roughness and OH fraction are directly related to the obtained adhesion strengths.

Fig. 10 presents the relative increase of (a) S_a and (b) OH fraction versus the relative increase in adhesion. From Fig. 10a it is observed that the relative increase of S_a of the 4000 grit surfaces is proportional to the increase in adhesion strength. Furthermore, for the 800 grit samples this proportionality is absent and a relative increase in adhesion strength of 200% is obtained despite any increase in S_a. However, in Fig. 10b it can be seen that the trend between the relative increase in adhesion and the relative increase in OH fraction of the different pre-treated surfaces is the same for both the 4000 grit and 800 grit series. The lowest relative increase of OH fraction and adhesion are obtained after HNO_3 pre-treatment, while the highest were obtained after boiling water pre-treatment. The correlation between the relative increases in OH fraction versus adhesion for the 800 grit samples agrees with the results from the Pearson correlation and t-distribution test and confirms OH fraction is the dominant variable.

4. Conclusions

The present study was devoted to investigate the dependence of the adhesion strength of an inorganic-organic hybrid sol-gel film deposited on commercially pure Al on the surface chemistry and surface roughness. The surface chemistry was altered using three different pre-treatments; nitric acid treatment (HNO_3), alkaline etch (KOH) and boiling DI water treatment, while surface morphology (roughness) was controlled with two different grinding procedures.

The main conclusions are as follows:

1. Pre-treatments have a considerable effect on the surface morphology of commercially pure fine abraded Al, while negligibly effect on the surface morphology of rougher Al.
2. The morphology is overall dominated by roughness intrinsically present and not by chemistry, caused by pre-treatment.
3. XPS spectra shows non-significant alterations of the overall surface elemental composition after the different pre-treatments
4. Surface hydroxyl-fraction increases considerably after all pre-treatments highest fractions are obtained after boiling water pre-treatment, which stems from pseudoboehmite formation.
5. Pre-treatments induce significant roughness changes, to the fine (4000 grit) samples, expressed by S_a and S_{sk}, and non-significant roughness changes to the rougher (800 grit) surfaces samples.
6. Water contact angle is largely affected by HNO_3 and KOH pre-treatments for 4000 grit, while water contact angle is only moderately affected by the pre-treatments for 800 grit.
7. The highest water contact angle was observed after HNO_3 and KOH pre-treatment as a result of a microporous structure (SEM), while the lowest was observed after boiling water pre-treatment, as a result of the formation of a pseudoboehmite layer.
8. Adhesion of an epoxy layer is largely affected by the application of a sol-gel layer and improves further with the pre-treatments, in particular after boiling DI water treatment. This is valid for both 4000 and 800 grit abraded surfaces.

9. Statistical analysis proved that both hydroxyl fraction and surface roughness are related with adhesion.
10. Hydroxyl fraction and surface roughness are not correlated with the water contact angle.
11. The strong correlation between hydroxyl fraction and adhesion strength evidences the effect of surface chemistry and efficient interactions across the aluminium/sol-gel interface on the properties of the sol-gel.

Declaration of Competing Interest

The authors declare that they have no known competing financial interests or personal relationships that could have appeared to influence the work reported in this paper.

Acknowledgements

This work was supported by the European Union's Horizon 2020 Research and Innovation Programme under the Marie Skłodowska-Curie Grant agreement No. 707404. J.P.B.D. acknowledges financial support by Materials Innovation Institute M2i and Technology Foundation TTW (www.stw.nl), which is part of the Netherlands Organization for Scientific Research under project number S32.4.14552b.

Appendix

Table A1, A2 A3
Fig. A1, A2 A3, A4, A5

References

[1] R.B. Figueira, C.J.R. Silva, E.V. Pereira, Organic–inorganic hybrid sol–gel coatings for metal corrosion protection: a review of recent progress, J. Coatings Technol. Res. 12 (2015) 1–35, https://doi.org/10.1007/s11998-014-9595-6.
[2] C. Carrera-Figueiras, Y. Pérez-Padilla, M. Alejandro Estrella-Gutiérrez, E.G. Uc-Cayetano, J. Antonio Juárez-Moreno, A. Avila-Ortega, Surface science engineering through sol-gel process, Appl. Surf. Sci., IntechOpen (2019), https://doi.org/10.5772/intechopen.83676.
[3] M. Guglielmi, Sol-gel coatings on metals, J. Sol-Gel Sci. Technol. 8 (1997) 443–449, https://doi.org/10.1007/BF02436880.
[4] R.B. Figueira, Hybrid sol–gel coatings for corrosion mitigation: a critical review, Polymers (Basel) 12 (2020) 689, https://doi.org/10.3390/polym12030689.
[5] R.B. Figueira, I.R. Fontinha, C.J.R. Silva, E.V. Pereira, Hybrid sol-gel coatings: Smart and green materials for corrosion mitigation, Coatings 6 (2016), https://doi.org/10.3390/coatings6010012.
[6] Z. Feng, Y. Liu, T. Hashimoto, G.E. Thompson, X. Zhou, P. Skeldon, Influence of surface pretreatments on the corrosion protection of sol-gel coated AA2024-T3 aluminium alloy, Surf. Interface Anal. 45 (2013) 1452–1456, https://doi.org/10.1002/sia.5216.
[7] A.A.C. Silva, T.I. Gomes, B.D.P. Martins, R.B.R. Garcia, L.D.S. Cividanes, E. Y. Kawachi, New insights in adhesive properties of hybrid epoxy-silane coatings for aluminum substrates: effect of composition and preparation methods, J. Inorg. Organomet. Polym. Mater. 30 (2020) 3105–3115, https://doi.org/10.1007/s10904-020-01468-y.
[8] S.T. Abrahami, Cr (VI)-Free Pre-Treatments For Adhesive Bonding Of Aerospace Aluminium Alloys, Delft University of Technology, 2016.
[9] S.Y. Park, W.J. Choi, H.S. Choi, A review of the recent developments in surface treatment techniques for bonded repair of aluminum airframe structures, Int. J. Adhes. Adhes. 80 (2018) 16–29, https://doi.org/10.1016/j.ijadhadh.2017.09.010.
[10] S.Y. Park, W.J. Choi, B.C. Yoon, Analysis of effects of process factors on corrosion resistance of adhesive bonded joints for aluminum alloys, J. Mater. Process. Technol. 276 (2020), 116412, https://doi.org/10.1016/j.jmatprotec.2019.116412.
[11] U. Tiringer, I. Milošev, A. Durán, Y. Castro, Hybrid sol–gel coatings based on GPTMS/TEOS containing colloidal SiO2 and cerium nitrate for increasing corrosion protection of aluminium alloy 7075-T6, J. Sol-Gel Sci. Technol. 85 (2018) 546–557, https://doi.org/10.1007/s10971-017-4577-7.
[12] Masume Masudi, A. Rahimi, R.P. Astaneh, Synthesis, characterization, and investigation of inhibitor release of the anticorrosion sol–gel hybrid nanocomposite coatings, Prot. Met. Phys. Chem. Surfaces 55 (2019) 363–370, https://doi.org/10.1134/S2070205119020205.
[13] U. Tiringer, A. Durán, Y. Castro, I. Milošev, Self-healing effect of hybrid sol-gel coatings based on GPTMS, TEOS, SiO 2 nanoparticles and Ce(NO 3) 3 applied on aluminum alloy 7075-T6, J. Electrochem. Soc. 165 (2018) C213–C225, https://doi.org/10.1149/2.0211805jes.
[14] A. Rahimi, S. Amiri, Self-healing hybrid nanocomposite coatings with encapsulated organic corrosion inhibitors, J. Polym. Res. 22 (2015) 624, https://doi.org/10.1007/s10965-014-0624-z.
[15] F. Brusciotti, A. Batan, I. De Graeve, M. Wenkin, M. Biessemans, R. Willem, F. Reniers, J.J. Pireaux, M. Piens, H.Terryn J.Vereecken, Characterization of thin water-based silane pre-treatments on aluminium with the incorporation of nano-dispersed CeO2 particles, Surf. Coatings Technol. 205 (2010) 603–613, https://doi.org/10.1016/j.surfcoat.2010.07.052.
[16] M.L. Zheludkevich, R. Serra, M.F. Montemor, M.G.S. Ferreira, Oxide nanoparticle reservoirs for storage and prolonged release of the corrosion inhibitors, Electrochem. Commun. 7 (2005) 836–840, https://doi.org/10.1016/j.elecom.2005.04.039.
[17] M.L. Zheludkevich, R. Serra, M.F. Montemor, K.A. Yasakau, I.M.M. Salvado, M.G. S. Ferreira, Nanostructured sol-gel coatings doped with cerium nitrate as pre-treatments for AA2024-T3 Corrosion protection performance, Electrochim. Acta 51 (2005) 208–217, https://doi.org/10.1016/j.electacta.2005.04.021.
[18] I. De Graeve, J. Vereecken, A. Franquet, T. Van Schaftinghen, H. Terryn, Silane coating of metal substrates: complementary use of electrochemical, optical and thermal analysis for the evaluation of film properties, Prog. Org. Coatings 59 (2007) 224–229, https://doi.org/10.1016/j.porgcoat.2006.09.006.
[19] A. Franquet, H. Terryn, J. Vereecken, Study of the effect of different aluminium surface pretreatments on the deposition of thin non-functional silane coatings, Surf. Interface Anal. 36 (2004) 681–684, https://doi.org/10.1002/sia.1735.
[20] R. Naderi, M. Fedel, T. Urios, M. Poelman, M.G. Olivier, F. Deflorian, Optimization of silane sol-gel coatings for the protection of aluminium components of heat exchangers, Surf. Interface Anal. 45 (2013) 1457–1466, https://doi.org/10.1002/sia.5249.
[21] J.S. Gandhi, W.J. Van Ooij, Improved corrosion protection of aluminum alloys by electrodeposited silanes, J. Mater. Eng. Perform. 13 (2004) 475–480, https://doi.org/10.1361/10599490420016.
[22] M. Fedel, Effect of sol–gel layers obtained from GLYMO/MTES mixtures on the delamination of a cataphoretic paint on AA1050, J. Coatings Technol. Res. 14 (2017) 425–435, https://doi.org/10.1007/s11998-016-9860-y.
[23] M. Fedel, F. Deflorian, Influence of a boiling water treatment on the electrochemical properties of a sol-gel film on AA1050, Trans. Inst. Met. Finish 93 (2015) 313–320, https://doi.org/10.1080/00202967.2015.1117261.
[24] F. Deflorian, M. Fedel, Effect of the surface chemical treatment on the properties of a sol–gel film on AA1050, Surf. Interface Anal. 48 (2016) 913–920, https://doi.org/10.1002/sia.5850.
[25] B. Arkles, J.R. Steinmetz, J. Zazyczny, P. Mehta, Factors contributing to the stability of alkoxysilanes in aqueous solution, J. Adhes. Sci. Technol. 6 (1992) 193–206, https://doi.org/10.1163/156856192X00133.
[26] M. Poberžnik, D. Costa, A. Hemeryck, A. Kokalj, Insight into the bonding of silanols to oxidized aluminum surfaces, J. Phys. Chem. C 122 (2018) 9417–9431, https://doi.org/10.1021/acs.jpcc.7b12552.
[27] K. Marcoen, M. Gauvin, J. De Strycker, H. Terryn, T. Hauffman, Molecular characterization of multiple bonding interactions at the steel oxide-aminopropyl triethoxysilane interface by ToF-SIMS, ACS Omega 5 (2020) 692–700, https://doi.org/10.1021/acsomega.9b03330.
[28] P.R. Underhill, A.N. Rider, Hydrated oxide film growth on aluminium alloys immersed in warm water, Surf. Coatings Technol. 192 (2005) 199–207, https://doi.org/10.1016/j.surfcoat.2004.10.011.
[29] J. Van den Brand, W.G. Sloof, H. Terryn, J.H.W. De Wit, Correlation between hydroxyl fraction and O/Al atomic ratio as determined from XPS spectra of aluminium oxide layers, Surf. Interface Anal. 36 (2004) 81–88, https://doi.org/10.1002/sia.1653.
[30] Ö. Özkanat, F.M. de Wit, J.H.W. de Wit, H. Terryn, J.M.C. Mol, Influence of pretreatments and aging on the adhesion performance of epoxy-coated aluminum, Surf. Coatings Technol. 215 (2013) 260–265, https://doi.org/10.1016/j.surfcoat.2012.07.096.
[31] J. Wielant, T. Hauffman, O. Blajiev, R. Hausbrand, H. Terryn, Influence of the iron oxide acid-base properties on the chemisorption of model epoxy compounds studied by XPS, J. Phys. Chem. C 111 (2007) 13177–13184, https://doi.org/10.1021/jp072354j.
[32] E. McCafferty, J.P. Wightman, Determination of the concentration of surface hydroxyl groups on metal oxide films by a quantitative XPS method, Surf. Interface Anal. 26 (1998) 549–564, https://doi.org/10.1002/(sici)1096-9918(199807)26:8<549::aid-sia396>3.3.co;2-h.
[33] J. Cerezo, I. Vandendael, R. Posner, J.H.W. de Wit, J.M.C. Mol, H. Terryn, The effect of surface pre-conditioning treatments on the local composition of Zr-based conversion coatings formed on aluminium alloys, Appl. Surf. Sci. 366 (2016) 339–347, https://doi.org/10.1016/j.apsusc.2016.01.106.
[34] J. van den Brand, P.C. Snijders, W.G. Sloof, H. Terryn, J.H.W. de Wit, Acid−Base characterization of aluminum oxide surfaces with XPS, J. Phys. Chem. B 108 (2004) 6017–6024, https://doi.org/10.1021/jp037877f.
[35] K.Y. Law, Definitions for hydrophilicity, hydrophobicity, and superhydrophobicity: getting the basics right, J. Phys. Chem. Lett. 5 (2014) 686–688, https://doi.org/10.1021/jz402762h.
[36] P. Schober, L.A. Schwarte, Correlation coefficients: Appropriate use and interpretation, Anesth. Analg. 126 (2018) 1763–1768, https://doi.org/10.1213/ANE.0000000000002864.
[37] G. James, D. Witten, T. Hastie, R. Tibshirani, An Introduction to Statistical Learning: with Applications in R, Springer New York, New York, 2013, https://doi.org/10.1007/978-1-4614-7138-7.
[38] M. Pourbaix, Atlas of Electrochemical Equilibria in Aqueous Solutions, 2nd ed., NACE International Cebelcor, Houston, Texas, 1974.
[39] B.V. Crist, Handbook of Monochromatic XPS Spectra, Semiconductors, Wiley-VCH, 2000.

[40] K. Patel, C.S. Doyle, D. Yonekura, B.J. James, Effect of surface roughness parameters on thermally sprayed PEEK coatings, Surf. Coatings Technol. 204 (2010) 3567–3572, https://doi.org/10.1016/j.surfcoat.2010.04.026.
[41] A. Noro, M. Kaneko, I. Murata, M. Yoshinari, Influence of surface topography and surface physicochemistry on wettability of zirconia (tetragonal zirconia polycrystal), J. Biomed. Mater. Res. Part B Appl. Biomater. 101 B (2013) 355–363, https://doi.org/10.1002/jbm.b.32846.
[42] C. Ishino, K. Okumura, Wetting transitions on textured hydrophilic surfaces, Eur. Phys. J. E 25 (2008) 415–424, https://doi.org/10.1140/epje/i2007-10308-y.
[43] A. Marmur, Wetting on hydrophobic rough surfaces: to be heterogeneous or not to be? Langmuir 19 (2003) 8343–8348, https://doi.org/10.1021/la0344682.
[44] S.T. Abrahami, T. Hauffman, J.M.M. de Kok, J.M.C. Mol, H. Terryn, Effect of anodic aluminum oxide chemistry on adhesive bonding of epoxy, J. Phys. Chem. C (2016), https://doi.org/10.1021/acs.jpcc.6b04957 acs.jpcc.6b04957.
[45] J. Cerezo, P. Taheri, I. Vandendael, R. Posner, K. Lill, J.H.W. de Wit, J.M.C. Mol, H. Terryn, Influence of surface hydroxyls on the formation of Zr-based conversion coatings on AA6014 aluminum alloy, Surf. Coatings Technol. 254 (2014) 277–283, https://doi.org/10.1016/j.surfcoat.2014.06.030.